ISSN (e): 2250 – 3005 || Vol, 05 || Issue, 01 || January – 2015 ||
International Journal of Computational

C^0 Mixed Layerwise Quadrilateral Plate Element with Variable in and Out-Of-Plane Kinematics and Fixed D.O.F.

Icardi U.[1], Sola F.[2]

[1]Associate Professor - Dipartimento di Ingegneria Meccanica e Aerospaziale
Politecnico di Torino - Corso Duca degli Abruzzi 24, 10129 Torino, Italy
Corresponding author. Tel: +39 (0)115646872; fax: +39 (0)115646899
[2]PhD Student - Dipartimento di Ingegneria Meccanica e Aerospaziale
Politecnico di Torino - Corso Duca degli Abruzzi 24, 10129 Torino, Italy

Abstract:
A quadrilateral, eight-node, mixed plate element based upon a recent 3D, variable kinematics zig-zag plate model by the authors is developed. Representation can be refined across the thickness though the number of unknown does not depend on the number of constituent layers, the nodal variables being fixed. The out-of-plane stress continuity is a priori satisfied at the interfaces and the material properties are allowed to step-vary moving over the plane of the structure. In order to obtain a C0 model, all derivatives of unknowns are converted with a technique that does not introduce additional d.o.f. Equilibrium equations are satisfied just in approximate integral form, mid-plane displacements and interlaminar stresses, the nodal d.o.f., being interpolated using the same standard serendipity shape functions. As shown by numerical results, this does not result in any precision loss. Accuracy, solvability and convergence are assessed considering multi-layered monolithic and sandwich-like structures with different boundary conditions and abruptly changing material properties across the thickness, for which exact solutions are available. Also a bonded joint is studied, which is treated as a laminate with spatially variable properties. In all these cases, the element is shown to be fast convergent and free from spurious, oscillating results.

Keywords: *partial hybrid formulation; intra-element equilibrium in an approximate integral form; fixed d.o.f.; hierarchic representation; C0 plate element;*

I. INTRODUCTION

Laminated and sandwich composites increasingly find use, as they enable design and construction of structures that achieve the target requirements with a lower mass than their metallic monolithic counterparts and they also offer the possibility to optimize the structural performances by properly choosing the fibre orientation and the stacking lay-up (see, e.g. Sliseris and Rocens [1]).

Manufacturing technologies such as automated fibre-placement (Barth [2]) pave the way to the spread of variable-stiffness composites in which the fibres follow curvilinear paths. Variable strength, stiffness and dissipation properties offer many advantages, as shown e.g. in Refs. [3] and [4], since the constituent materials can be designed using advanced optimization techniques for keeping maximal the overall performance parameters. At the same time, it is possible to relax the critical local stress concentrations inherent to the inhomogeneous microstructure of composites that give rise to damage. A recent, comprehensive discussion of the mechanisms of damage formation and evolution of composites and of their modelling is given by Càrdenas et al. [5].

Since the local damage can have very harmful effects, the simulations should accurately account for the stress fields responsible of the damage rise and growth, their strong concentrations at the interfaces, their effects on strength, stiffness and durability and the warping, shearing and straining deformations of the normal produced by the material discontinuities and the much bigger elastic moduli and strengths in the in-plane direction compared to those in the thickness. These so called zig-zag and layerwise effects should be described into details but with an affordable computational effort, as discussed by Chakrabarti et al. [6], Qatu et al. [7] and Zhang and Yang [8].

Displacement-based models and related finite elements should feature appropriate discontinuous derivatives of displacements in the thickness direction at the interfaces, while mixed models should assume appropriate continuous, self-equilibrated stresses. Composite plate and shell theories and elements satisfying

these requirements have been developed either in displacement-based or mixed form using different approaches. Displacement-based finite elements require fine meshes and a large computational effort to accurately determine stresses, since they are obtained from displacements (constitutive equations) or from in-plane stresses (integration of local equilibrium equations), thus accuracy deteriorates. Mixed/hybrid models and elements offer the advantage of a more easily enforcement of interfacial and boundary constraints, the stresses being treated as primary variables separately from displacements. Moreover, they provide more accurate results than displacement-based models with the same meshing and with a comparable processing time, as shown in the literature. On the other hand stability, convergence and solvability are more complex than those of their displacement-based counterparts.

An extensive discussion of the various techniques used to account for the layerwise effects and extensive assessments of their structural performances are presented by Chakrabarti et al. [6], Matsunaga [9], Chen and Wu [10], Kreja [11], Tahani [12] and Gherlone [13]. Accuracy of finite element models for layered and sandwich composites is assessed by Carrera et al. [14]. Finite element models are also discussed in the papers by Chakrabarti et al. [6], Zhang and Yang [8], Shimpi and Ainapure [15], Elmalich and Rabinovitch [16], Dau et al. [17] and for what concerns mixed/hybrid methods in the book by Hoa and Feng [18], and in the papers by Feng and Hoa [19], Desai et al. [20], Ramtekkar et al. [21] and To and Liu [22]. Recent examples of finite elements for analysis of composites are those by Zhen et al [23], Cao et al. [24] (hybrid formulation) and Dey at al. [25].

Accuracy and computational costs of layerwise models and elements can considerably vary, depending on their number of unknowns. A separate representation in any computational layer results in a high accuracy (see, e.g. Reddy [26]), but since the number of variables increases with the number of physical/computational layers, computational costs can become unaffordable when analysing structures of industrial complexity. Models based on a combination of global higher-order terms and local layerwise functions are often used for analysis of composites, as they have been proven to be equally accurate with a much lower computational effort (see, e.g. Elmalich and Rabinovitch [16] and the references therein cited). The zig-zag models inspired by Di Sciuva [27] have also found many applications and related finite elements are widespread, being low cost partial layerwise models with just the three mid-plane displacements and the two transverse shear rotations as functional d.o.f., like equivalent single-layer models. Physically-based continuity functions are incorporated in the displacement field in order to a priori satisfy the continuity of out-of-plane stresses at the layer interfaces, whose expressions are determined once for all. Initially, just the piecewise variation of in-plane displacements across the thickness was considered, the transverse displacement being assumed constant. Refinements have been brought over years in order to incorporate a variable transverse displacement, since it has a significant bearing for keeping equilibrium in certain cases. A great amount of research work was also done to successfully treat panels with low length-to thickness ratio and abruptly changing material properties, like sandwiches, which can be described as multi-layered structures whenever a detailed description of local phenomena in the cellular structure is unnecessary [28]. Sublaminate models having top and bottom face d.o.f. were developed in order to stack computational layers [29]. The displacement field was recast in a global-local form to accurately predict stresses from constitutive equations (see, Li and Liu [30], Zhen and Wanji [31]), though at the expense of a larger number of functional d.o.f., because post-processing operations are unwise for finite elements and cannot always be precise [32].

As a result of these refinement studies, to date zig-zag models and elements offer a good accuracy with the lowest computational burden. Regrettably, derivatives of the functional d.o.f. are involved by such physically-based zig-zag models, and consequently they should appear as nodal d.o.f. in the finite elements, implying to use C1 or high-order interpolation functions with a lower computational efficiency than C0ones. Techniques such those proposed by Zhen and Wanji [31] and Sahoo and Singh [33] could be employed for converting derivatives, but they result in an increase of the nodal d.o.f and thus of the memory storage dimension. The Murakami's zig-zag function just based upon kinematic assumptions is often used as local layerwise function since it overcomes the problem and it is much easier to implement than the physically consistent zig-zag functions, though it is not always equally accurate. The assessments carried out by Gherlone [13] proven that Murakami's zig-zag is accurate for periodical stack-ups, but not for laminates with arbitrary stacking sequences, or for asymmetrical sandwiches with high face-to-core stiffness ratios, like when a weak layer is placed on the top or bottom to simulate a damaged face.

Aimed at carrying out the analysis of multi-layered and sandwich composites having abruptly changing material properties with the minimal computational burden, the recently developed physically-based zig-zag model of Ref. [34] was developed assuming a through-the-thickness variable representation of displacements that can be locally refined like for discrete layer models, though its functional d.o.f. are fixed (the classical displacements and shear rotations of the normal at the mid-plane). A high-order piecewise zig-zag variation of all the displacements was assumed in order to account for the core's crushing behaviour of sandwiches, for keeping equilibrium at cut-outs, free edges, nearby material/geometric discontinuities and to

predict stresses caused by temperature gradients, because in these cases the piecewise variation of the transverse displacement is as important as that of its in-plane counterparts (see, e.g. [23] and [35]). The physical constraints, i.e. the interfacial stress contact conditions, stress boundary conditions at the bounding faces and the indefinite equilibrium equations at selected points across the thickness were satisfied without increasing the number of unknown variables because symbolic calculus was used to obtain automatically and once for all relations in closed-form as functions of the assumed five d.o.f. Accurate results were obtained in numerical applications with a computational effort considerably lower than for other layerwise models, thus model [34] is of practical interest toward development of finite elements.

In the present paper, the energy updating technique of Refs. [36] – [38], here referred as SEUPT, is used to convert derivatives without resulting in an increased number of nodal variables. SEUPT was originally developed as an iterative post-processing technique for improving the predictive capability of shear deformable commercial finite plate elements. The present revised version of SEUPT consists of a technique that allows obtainment of an equivalent C0 version (EM model) of the zig-zag model [34] by the energy standpoint, which is used to develop an efficient plate element in mixed form having the displacements and the interlaminar stresses at the reference mid-plane as nodal d.o.f. A priori corrections of displacements are obtained in closed-form through SEUPT using symbolic calculus by making the energy of the model [34] free from derivatives equal to that of its counterpart containing all the derivatives. Hermite's polynomials are assumed in the energy balance equations for the consistent zig-zag model, while Lagrange's polynomials are used for the equivalent counterpart model free from d.o.f. derivatives. The equivalent C0 displacement fields and the out-of-plane stresses derived in this way are used to develop the present mixed element. It is a partial hybrid one, because, according to Ref. [19], it only includes out-of-plane stresses as nodal d.o.f., just these stresses having to be continuous across the material interfaces and being essential for analysis of composites. The stresses by the EM model are modified adding new continuity functions that restore the equilibria at the interfaces, because stress continuity could be lost in the equivalent model.

Displacement and stress interpolating functions all of the same order are considered, the same C0 interpolation by standard serendipity polynomials being used for all the nodal d.o.f. , so the intra element equilibrium equations are satisfied just in an approximate integral form. This option was chosen because it reduces the effort for developing the element without losing accuracy, as shown in the pioneering paper by Loubignac et al. [39] and in the book by Nakazawa [40].

Accuracy, solvability and convergence behaviour of the present mixed element will be assessed comparing its results for laminates and sandwiches with different boundary conditions and abruptly changing material properties with the exact solutions computed with the technique by Pagano [41]. The sample cases by Zhen et al. [23], Vel and Batra [42], Icardi [43], Brischetto et al. [44], Tessler et al. [45] and Robbins and Reddy [46] are considered. As an application to a practical case, the stress field of a double lap joint computed by the present mixed element is compared to the exact solution by Nemes and Lachaud [47].

The paper is structured as follows. First, the basic features of the zig-zag plate model are overviewed. Then, SEUPT is recast in a form suited for the present element. Finally, the element is developed and applied to the analysis of sample cases.

II. STRUCTURAL MODEL

A rectangular Cartesian reference frame (x, y, z) with (x, y) on the middle surface of the plate (Ω) and z normal to it is assumed as reference system. The displacement field is assumed as the as the sum of four separated contributions:

$$\begin{aligned} u(x,y,z) &= U^0(x,y,z)+U^i(x,y,z)+U^c(x,y,z)+U^{c-ip}(x,y,z) \\ v(x,y,z) &= V^0(x,y,z)+V^i(x,y,z)+V^c(x,y,z)+V^{c-ip}(x,y,z) \\ w(x,y,z) &= W^0(x,y,z)+W^i(x,y,z)+W^c(x,y,z)+W^{c-ip}(x,y,z) \end{aligned} \tag{1}$$

Here the symbols u, v and w respectively define the elastic displacements in the directions x, y and z.

The first three contributions are the same of the model developed in Ref. [34], the latter one was added in Ref. [38] to treat properties and/or lay-up suddenly varying in x, y directions, like across adherends and overlap of bonded joints.

2.1 Basic contribution Δ^0

The basic contributions, indicated with superscript ^{0} or in compact form as Δ^0, repeat the kinematics of the FSDPT model, thus they contain just a linear expansion in z:

$$\begin{aligned} U^0(x,y,z) &= u^0(x,y)+z\left[\gamma_x^0(x,y)-w^0{}_{,x}(x,y)\right] \\ V^0(x,y,z) &= v^0(x,y)+z\left[\gamma_y^0(x,y)-w^0{}_{,y}(x,y)\right] \end{aligned} \tag{2}$$

$$W^0(x,y,z) = w^0(x,y)$$

Eq. (2) is well known and it has been used in many applications, therefore it does not need further explanations. Here it is only reminded that the displacements $u^0(x, y)$, $v^0(x, y)$, $w^0(x, y)$ and the transverse shear rotations at the middle plane $\gamma_x{}^0(x, y)$ and $\gamma_y{}^0(x, y)$ represent the five functional d.o.f.

2.2 Variable kinematics contribution Δ^i

The contributions with superscript ^{i}, indicated in compact form with the symbol Δ^i, allow the model adapting to local variation of solutions, enabling a refinement across the thickness. Therefore these contributions have a representation that can vary from point to point across the thickness:

$$\begin{aligned} U^i(x,y,z) &= A_{x1}z + A_{x2}z^2 + A_{x3}z^3 + A_{x4}z^4 + \ldots + A_{xn}z^n \\ V^i(x,y,z) &= A_{y1}z + A_{y2}z^2 + A_{y3}z^3 + A_{y4}z^4 + \ldots + A_{yn}z^n \\ W^i(x,y,z) &= A_{z1}z + A_{z2}z^2 + A_{z3}z^3 + A_{z4}z^4 + \ldots + A_{zn}z^n \end{aligned} \tag{3}$$

The unknown coefficients $A_{x1}\ldots A_{zn}$ are computed by enforcing the conditions:

$$\sigma_{xz}\,|^u = 0 \quad \sigma_{xz}|_l = 0 \tag{4}$$

$$\sigma_{yz}\,|^u = 0 \quad \sigma_{yz}|_l = 0 \tag{5}$$

$$\sigma_{zz}\,|^u = p^0\,|^u \quad \sigma_{zz}|_l = p^0\,|_l \tag{6}$$

$$\sigma_{zz,z}\,|^u = 0 \quad \sigma_{zz,z}|_l = 0 \tag{7}$$

and the equilibrium at discrete points across the thickness:

$$\begin{aligned} &\sigma_{xx,x} + \sigma_{xy,y} + \sigma_{xz,z} = 0 \\ &\sigma_{xy,x} + \sigma_{yy,y} + \sigma_{yz,z} = 0 \\ &\sigma_{xz,x} + \sigma_{yz,y} + \sigma_{zz,z} = 0 \end{aligned} \tag{8}$$

The symbols $^{(k)}z^+$ and $^{(k)}z^-$ indicate the position of the upper$^+$ and lower $^-$ surfaces of the kth layer, while the superscript(k) designates the quantities that belong to a generic layer k. As customarily, a comma is used to indicate differentiation. Please notice that the expressions of the unknowns $A_{x1}\ \ldots\ A_{zn}$ are computed through automatic, symbolic calculus (MATLAB® symbolic software package) without any increase in the number of unknowns, being obtained in closed-form as functions of the d.o.f. and of their derivatives. Contributions (3) neither results into a considerably larger computational effort, nor into a larger memory storage dimension, because irrespectively of the number of points chosen, the number of d.o.f. is fixed because the constraint relations are obtained in closed-form once for all just in terms of the variables $u^0(x, y)$, $v^0(x, y)$, $w^0(x, y)$, $\gamma_x{}^0(x, y)$, $\gamma_y{}^0(x, y)$ and of their derivatives. Because derivatives are unwise for the development of finite elements, they will be converted with the technique described forward.

2.3 Zig-zag piecewise contribution Δ^c

The piecewise terms Δ^c, which constitutes the zig-zag contributions, are assumed as follows:

$$\begin{aligned} U^c(x,y) &= \sum_{k=1}^{n_i} \Phi_x^k(x,y)(z-z_k)H_k + \sum_{k=1}^{n_i} C_u^k(x,y)H_k \\ V^c(x,y) &= \sum_{k=1}^{n_i} \Phi_y^k(x,y)(z-z_k)H_k + \sum_{k=1}^{n_i} C_v^k(x,y)H_k \\ W^c(x,y) &= \sum_{k=1}^{n_i} \Psi^k(x,y)(z-z_k)H_k + \sum_{k=1}^{n_i} \Omega^k(x,y)(z-z_k)^2 H_k + \sum_{k=1}^{n_i} C_w^k(x,y)H_k \end{aligned} \tag{9}$$

The terms of Eq. (9) make the displacements continuous and with appropriate discontinuous derivatives in the thickness direction at the interfaces of physical/computational layers, thus allowing to a priori fulfil the continuity of interlaminar stresses at the material interfaces. In details, terms $\Phi_x{}^k$, $\Phi_y{}^k$ are incorporated in order to satisfy:

$$\begin{aligned} \sigma_{xz}\,|_{(k)\,z^+} &= \sigma_{xz}\,|_{(k)\,z^-} \\ \sigma_{yz}\,|_{(k)\,z^+} &= \sigma_{yz}\,|_{(k)\,z^-} \end{aligned} \tag{10}$$

while Ψ_k, Ω_k are computed by enforcing the following continuity conditions:

$$\sigma_z|_{(k)_{z^+}} = \sigma_z|_{(k)_{z^-}}$$
$$\sigma_{z,z}|_{(k)_{z^+}} = \sigma_{z,z}|_{(k)_{z^-}} \tag{11}$$

which directly derive from the local equilibrium equations as a consequence of the continuity of transverse shear stresses.

The continuity of displacements at the points across the thickness where the representation is varied is restored by the functions C_u^k, C_v^k and C_w^k, whose expressions are computed imposing:

$$u\Big|_{(k)_{z^+}} = u\Big|_{(k)_{z^-}}$$
$$v\Big|_{(k)_{z^+}} = v\Big|_{(k)_{z^-}} \tag{12}$$
$$w\Big|_{(k)_{z^+}} = w\Big|_{(k)_{z^-}}$$

2.4 Variable in-plane representation Δ^{c_ip}

Differently to [34], it is supposed that the in-plane representation of displacements can vary, consequently to a sudden change of the material properties moving along the x or y direction. To this purpose, contributions Δ^{c_ip} are incorporated in a form similar to that used in [38]:

$$U^{c\_ip} = \sum_{j=1}^{S}\sum_{k=1}^{T} {}_u^j\theta_x^k(x,y)(x-x_k)H_k + \sum_{j=1}^{S}\sum_{k=1}^{T} {}_u^j\theta_y^k(x,y)(y-y_k)H_k + \sum_{j=1}^{S}\sum_{k=1}^{T} {}_u^j\lambda_x^k(x,y)(x-x_k)^2H_k + \sum_{j=1}^{S}\sum_{k=1}^{T} {}_u^j\lambda_y^k(x,y)(y-y_k)^2H_k + \ldots \tag{13}$$

$$V^{c\_ip} = \sum_{j=1}^{S}\sum_{k=1}^{T} {}_v^j\theta_x^k(x,y)(x-x_k)H_k + \sum_{j=1}^{S}\sum_{k=1}^{T} {}_v^j\theta_y^k(x,y)(y-y_k)H_k + \sum_{j=1}^{S}\sum_{k=1}^{T} {}_v^j\lambda_x^k(x,y)(x-x_k)^2H_k + \sum_{j=1}^{S}\sum_{k=1}^{T} {}_v^j\lambda_y^k(x,y)(y-y_k)^2H_k + \ldots \tag{13}'$$

In Eqs. (13) and (13)' the exponent of $(x - x_k)^n$, $(y - y_k)^n$ is chosen in order to make continuous the stress gradient of order *n*. For instance, the continuity conditions $\sigma_{xx}|_{(k)x+} = \sigma_{xx}|_{(k)x-}$, $\sigma_{yy}|_{(k)x+} = \sigma_{yy}|_{(k)x-}$ and $\sigma_{zz}|_{(k)x+} = \sigma_{zz}|_{(k)x-}$ require just first order terms of $(x - x_k)$, while the continuity of gradients $\sigma_{xx,x}|_{(k)x+} = \sigma_{xx,x}|_{(k)x-}$, $\sigma_{yy,x}|_{(k)x+} = \sigma_{yy,x}|_{(k)x-}$ and $\sigma_{zz,x}|_{(k)x+} = \sigma_{zz,x}|_{(k)x-}$ requires second order terms $(x - x_k)^2$, while higher-order gradients require the higher order contributions omitted in previous equations. The continuity functions appearing in (13), (13)' are computed in a straightforward way by enforcing previous conditions.

III. ENERGY UPDATING TECHNIQUE

Equivalent forms of models by the energy standpoint can be constructed using energy-based weak form versions of governing equations. As shown in [36] and [37], an iterative post-processing technique working on a spline interpolation of FEA result can be used to construct an updated solution that locally improves the accuracy of a finite element analysis carried out using standard shear-deformable plate elements. As shown in [38], a modified expression of the displacements field by a structural model that is free from derivatives of the functional d.o.f. can be constructed in order to obtain a C0 equivalent model without any additional d.o.f. using symbolic calculus to obtain once for all the relations in closed-form. The comparison with exact solutions of sample test cases demonstrated that the equivalent model (EM) can provide equally accurate results than the original model (OM), even when the through-the-thickness stress distributions are rather intricate. This opens the possibility of developing an efficient finite element free from nodal derivatives of the d.o.f.

Hereafter, the technique developed in [38] is retaken and revised with the aim of constructing a version of SEUPT that produces an equivalent zig-zag model suited to develop an efficient and accurate mixed plate element for analysis of laminated and sandwich composites.

3.1 Equivalent zig-zag model

The basic assumption of SEUPT is that each displacement of the OM model appearing in Eq. (1), hereon indicated as $u(x, y, z)^{OM}$, $v(x, y, z)^{OM}$, $w(x, y, z)^{OM}$ (superscript ^{OM} will define all the quantities that refer to this model) can be reconstructed using energy equivalence concepts, so that all the derivatives of the functional d.o.f. can be replaced. The objective is to derive modified expressions of the displacements, i.e. u(x,

$u(x, y, z)^{EM}$, $v(x, y, z)^{EM}$, $w(x, y, z)^{EM}$ (superscript ^{EM} will refer to the equivalent model) that will be used within each energy integral, so to have the energy functional free from derivatives.

It is assumed that the displacements of the OM model (in compact form $\forall^{OM}$) can be recast as the sum of a part $\forall^{\varnothing}$ free from derivatives of the d.o.f. and terms $\forall^{\cup}$ containing the derivatives

$$\forall^{OM}(x,y,z) = \forall^{\varnothing}(x,y,z) + \forall^{\cup}(x,y,z) \tag{14}$$

The basic assumption of SEUPT is that each term $\forall^{\cup}$ can be replaced incorporating corrective terms that are free from derivatives Δu^0, Δv^0, Δw^0, $\Delta \gamma_x{}^0$, $\Delta \gamma_y{}^0$ (in compact form $\Delta \forall^{\varnothing}$)

$$\forall^{EM}(x,y,z) = \forall^{\varnothing}(x,y,z) + \Delta\forall^{\varnothing}(x,y,z) \tag{14'}$$

whose expressions are derived from the energy balance

$$\delta\int(.)|_E = \delta\int(.)|_{\Lambda i} - \delta\int(.)|_{\Lambda f} + \delta\int(.)|_{\Lambda m} = 0 \tag{15}$$

in order to be equivalent by the energy standpoint. The principle of virtual works accounting for inertial forces is here used as the energy balance, but any other equivalent canonical functional could be successfully employed. As customarily, the symbols $\{\sigma_{ij}\}$ and $\{\varepsilon_{ij}\}$ represent the strain and stress vectors, respectively, b_i and t_i are the body and surface forces, ρ is the density and u_i are the displacements. The expressions of corrective terms $\Delta\forall^{\varnothing}$ are specific for any sub-integral constituting the virtual variations of the strain energy $\int(.)|_{\Lambda i} = \frac{1}{2}\int_V \{\sigma_{ij}\}^T \{\varepsilon_{ij}\} dV$, work of external forces $\int(.)|_{\Lambda f} = \int_V b_i u_i dV + \int_S t_i u_i dS$ and work of inertial forces $\int(.)|_{\Lambda m} = \int_V -\rho \ddot{u}_i u_i \, dV$ Therefore, each corrective term is computed by splitting the energy balance into five independent balance equations, here indicated in compact form as

$$\left[\delta\int(.)|_E\right]^{u^0} = 0;\ \left[\delta\int(.)|_E\right]^{v^0} = 0;\ \left[\delta\int(.)|_E\right]^{w^0} = 0;\ \left[\delta\int(.)|_E\right]^{\gamma_x{}^0} = 0;\ \left[\delta\int(.)|_E\right]^{\gamma_y{}^0} = 0; \tag{16}$$

i.e. one for each primary variable δu^0, δv^0, δw^0, $\delta \gamma_x{}^0$, $\delta \gamma_y{}^0$, and then further splitting into all sub-integrals $\delta\int(.)|_{E\longrightarrow}$ that added together form the five separate contributions (16) (i.e. $\Sigma\delta\int(.)|_{E\longrightarrow} = \delta\int(.)|_E$)

Different corrective terms Δu^0, Δv^0, Δw^0, $\Delta \gamma_x{}^0$, $\Delta \gamma_y{}^0$ are computed for each sub-integral $\delta\int(.)|_{E\longrightarrow}$ by imposing the result by the OM model to be equal by the energy standpoint to its counterpart by the EM model, in symbols:

$$\begin{aligned}
&\left[\delta\int(.)|_{E\longrightarrow}\right]^{u^0 OM} = \left[\delta\int(.)|_{E\longrightarrow}\right]^{u^0 EM} = 0;\\
&\left[\delta\int(.)|_{E\longrightarrow}\right]^{v^0 OM} = \left[\delta\int(.)|_{E\longrightarrow}\right]^{v^0 EM} = 0;\\
&\left[\delta\int(.)|_{E\longrightarrow}\right]^{w^0 OM} = \left[\delta\int(.)|_{E\longrightarrow}\right]^{w^0 EM} = 0;\\
&\left[\delta\int(.)|_{\longrightarrow E}\right]^{\gamma_x{}^0 OM} = \left[\delta\int(.)|_{E\longrightarrow}\right]^{\gamma_x{}^0 EM} = 0;\\
&\left[\delta\int(.)|_{E\longrightarrow}\right]^{\gamma_y{}^0 OM} = \left[\delta\int(.)|_{E\longrightarrow}\right]^{\gamma_y{}^0 EM} = 0;
\end{aligned} \tag{17}$$

The displacement fields are described as Hermite polynomials within the sub-integrals with the superscript ^{OM}, while Lagrange polynomials are used within sub- integrals with the superscript ^{EM}, because the functional d.o.f. and their derivatives should be assumed as nodal d.o.f. whether a conforming element is derived by the OM model, while no derivatives are required for an element derived by the EM model, as in the current case. At least third order derivatives are involved by the OM model as a consequence of the enforcement of the interfacial stress continuity and of the stress boundary conditions, but higher order derivatives could be involved enforcing additional conditions.

Representing each functional d.o.f. (i.e. $u^0(x,y)$, $v^0(x,y)$, $w^0(x,y)$, $\gamma_x^0(x,y)$, $\gamma_y^0(x,y)$) in compact form with the symbol $\wp$, the inner representation of variables of the OM model is expressed as the sum of tensor products of Hermite's polynomials ${}^{\rho}\mathrm{H}_i$ in *x* and *y* of the following form (index i represents the nodes numbering):

$$\wp = \sum_{i=1}^{4} {}^{\wp}\mathrm{H}_i \ \wp_i + \sum_{i=1}^{4} {}^{\wp,x}\mathrm{H}_i \ \wp_{i,x} + \sum_{i=1}^{4} {}^{\wp,y}\mathrm{H}_i \ \wp_{i,y} + \sum_{i=1}^{4} {}^{\wp,xx}\mathrm{H}_i \ \wp_{i,xx} + \sum_{i=1}^{4} {}^{\wp,xy}\mathrm{H}_i \ \wp_{i,xy} + \sum_{i=1}^{4} {}^{\wp,yy}\mathrm{H}_i \ \wp_{i,yy} + ... \tag{18}$$

Explicit terms have been reported in Eq. (18) only up to the second order of derivation, but higher-order terms could be included since the order of the interpolating functions is a direct consequence of the order of derivation, which in turns depends on the type of physical constraints enforced.

No derivatives are involved within sub-integrals $\left[\delta\int(.)|_{E\longrightarrow}\right]^{EM}$, because the EM model is a C^0 model. Hence, a computationally efficient Lagrangian representation can be used for the EM model, the same discussed forward to develop the present finite element.

The corrective displacements are obtained from Eq. (17) as functions of the nodal unknowns using symbolic calculus. Their expressions hold irrespectively of the loading and boundary conditions, lay-up and geometry. Being obtained once for all in closed-form, they consistently speed up computations.

Former balance equations (17) state that since the consistent displacement field by the OM model satisfies the energy balance, the modified displacements by the EM model satisfy it too, thus they represent an admissible solution by the energy standpoint. Because the EM model is just equivalent form the energy standpoint to the OM model, not in a point form, it just provides a correct solution in terms of displacements, but it could be unable to satisfy all the boundary constraints in a point-wise sense. In particular, the continuity of displacement derivatives and stresses at nodes and sides could not be identically satisfied by the Lagrangian representation used within the EM model. On the contrary, it can be satisfied by the Hermitian representation used for the OM model and by a suited definition of contributions Δ^c, Δ^{c_ip} to displacements. Hence, the EM model just provides the solution in terms of displacement d.o.f. at any point, while all the quantities that contain derivatives, like the stresses, should be determined by the OM model using the analytic expressions obtained through symbolic calculus. These operations are indicated in compact form as:

$$\begin{aligned}
&\left[\delta\int(.)|_E\right]^{u^0EM} \rightarrow \left[\delta\int(.)|_E\right]^{u^0OM};\\
&\left[\delta\int(.)|_E\right]^{v^0EM} \rightarrow \left[\delta\int(.)|_E\right]^{v^0OM};\\
&\left[\delta\int(.)|_E\right]^{w^0EM} \rightarrow \left[\delta\int(.)|_E\right]^{w^0OM};\\
&\left[\delta\int(.)|_E\right]^{\gamma_x{}^0EM} \rightarrow \left[\delta\int(.)|_E\right]^{\gamma_x{}^0OM};\\
&\left[\delta\int(.)|_E\right]^{\gamma_y{}^0EM} \rightarrow \left[\delta\int(.)|_E\right]^{\gamma_y{}^0OM};
\end{aligned} \tag{19}$$

These energy balance equations could be used as a post-processing technique for obtaining a progressively refined solution from the results of a preliminary finite element analysis:

$$\begin{aligned}
&\left[\delta\int(.)|_E\right]^{u^0EM} \Leftrightarrow \left[\delta\int(.)|_E\right]^{u^0OM};\\
&\left[\delta\int(.)|_E\right]^{v^0EM} \Leftrightarrow \left[\delta\int(.)|_E\right]^{v^0OM};\\
&\left[\delta\int(.)|_E\right]^{w^0EM} \Leftrightarrow \left[\delta\int(.)|_E\right]^{w^0OM};\\
&\left[\delta\int(.)|_E\right]^{\gamma_x{}^0EM} \Leftrightarrow \left[\delta\int(.)|_E\right]^{\gamma_x{}^0OM};\\
&\left[\delta\int(.)|_E\right]^{\gamma_y{}^0EM} \Leftrightarrow \left[\delta\int(.)|_E\right]^{\gamma_y{}^0OM};
\end{aligned} \tag{20}$$

like in the former applications of SEUPT, but this is not of interest in this paper. Instead, the objective is the obtainment of accurate results without any post-processing operation. Indeed, Eqs. (19) and (20) are fast carried out using expressions obtained through symbolic calculus, but they however result in an increased

computational burden. A mixed element is developed to overcome the use of Eqs. (19), (20) as the stresses, which are interpolated separately from displacements, are predicted very accurately. The interlaminar stresses that are the ones critical by the viewpoint of strength, stiffness and durability are assumed as nodal d.o.f.

In order to enable the development of such a mixed element, the interlaminar stresses computed by the equivalent displacements of the EM model, here indicated as $\hat{\sigma}^{J}_{xz}$, $\hat{\sigma}^{J}_{yz}$ $\hat{\sigma}^{J}_{yz,}$ are modified incorporating unknown continuity functions $\Lambda^{(k)}$

$$\sigma_{xz}^{J} = \hat{\sigma}_{xz}^{J} + \sum_{k=1}^{S} \Lambda^{(k)} H_k \tag{21}$$

$$\sigma_{yz}^{J} = \hat{\sigma}_{yz}^{J} + \sum_{k=1}^{S} \Theta^{(k)} H_k \tag{22}$$

$$\sigma_{zz}^{J} = \hat{\sigma}_{zz}^{J} + \sum_{k=1}^{S} \Gamma^{(k)} H_k \tag{23}$$

That make continuous the stresses σ^{J}_{xz}, σ^{J}_{yz}, σ^{J}_{zz} at the layer interfaces

$$\sigma_{xz}^{J(+)} = \hat{\sigma}_{xz}^{J(-)} \quad \sigma_{yz}^{J(+)} = \hat{\sigma}_{yz}^{J(-)} \quad \sigma_{zz}^{J(+)} = \hat{\sigma}_{zz}^{J(-)} \tag{24}$$

The new continuity functions appearing in (21)-(23) are computed in a straightforward way since now they are not expressed in terms of displacements as before (9), thus no derivatives are involved, differently from [38] where the stresses were obtained from the displacements. Accordingly, their in-plane variation can be assumed in Lagrangian form like for the displacement d.o.f. In the present element, the mid-plane stresses are assumed as stress d.o.f. Once the finite element solution has been found, their variation across the thickness is computed by the constitutive equations (21)-(23) at any z.

It could be noticed that for keeping the model in C^0 form, the continuity of the transverse normal stress $\sigma^{J}_{zz,z}{}^{(+)} = \sigma^{J}_{zz,z}{}^{(-)}$ appearing in Eq. (11) has been disregarded in Eq. (24). In order to indirectly fulfil this necessary condition, the interlaminar stresses of the EM model are made consistent with those of the OM model that fulfil (11) by further enforcing the equivalence conditions

$$\begin{aligned}
\left[\int (\sigma_{xz}\delta\varepsilon_{xz})|_{E\longrightarrow}\right]^{OM} &= \left[\delta\int ((\sigma_{xz}+\Delta\sigma_{xz})\delta\varepsilon_{xz})|_{E\longrightarrow}\right]^{EM};\\
\left[\int (\sigma_{yz}\delta\varepsilon_{yz})|_{E\longrightarrow}\right]^{OM} &= \left[\delta\int ((\sigma_{yz}+\Delta\sigma_{yz})\delta\varepsilon_{yz})|_{E\longrightarrow}\right]^{EM};\\
\left[\int (\sigma_{zz}\delta\varepsilon_{zz})|_{E\longrightarrow}\right]^{OM} &= \left[\delta\int ((\sigma_{zz}+\Delta\sigma_{zz})\delta\varepsilon_{zz})|_{E\longrightarrow}\right]^{EM}
\end{aligned} \tag{25}$$

from which the corrective stresses $\Delta\sigma_{xz}$, $\Delta\sigma_{yz}$, $\Delta\sigma_{zz}$ are computed in closed-form once for all again using symbolic calculus. The Hermitian representation for the OM model and a Lagrangian one for the EM model are still used.

3.2 Finite element

Based on the updated version of SEUPT discussed above, an eight-node mixed plate element with standard Lagrangian interpolating functions is developed. The terms mixed is used to indicate that the master fields are internal fields. As nodal d.o.f. the nodal components of displacements $u(x,y,z)^{EM}$, $v(x,y,z)^{EM}$, $w(x,y,z)^{EM}$ and the stresses σ_{xz}^{J}, σ_{yz}^{J}, σ_{zz}^{J} at the reference middle plane are assumed (see Figure 1a), as mentioned above. In this way, only the continuity of interlaminar stresses is considered. It should be noticed that the continuity of stress components parallel to an interface should not be forced, being physically incorrect for multi-layered structures.

Since stresses and displacements can be varied separately, the Hellinger-Reissner multi-field principle:

$$\delta\Pi_{HR} = \delta\int_V \sigma_{ij}\varepsilon_{ij}^{u} - \frac{1}{2}\sigma_{ij}S_{ijkl}\sigma_{kl}dV - \delta\left(\int_V b_i u_i dV + \int_S t_i u_i dS\right) = \delta U_{HR} - \delta W_{HR} \tag{26}$$

is the governing functional. The symbol S_{ijkl} represent the components of the elastic compliance tensor, the inverse of the elastic stiffness tensor C_{ijkl}, so that $S_{ijkl}\ \sigma_{kl} = \varepsilon_{ij}^{\sigma}$ represents the strains obtained from the stress-strain relations

Accordingly, ½ $\sigma_{ij}\ S_{ijkl}\ \sigma_{kl}$ represents the complementary energy density in term of the master stress field. The slave fields are the strains $\varepsilon_{ij}^{\sigma}$ and ε_{ij}^{u}:

$$\varepsilon^{\sigma}{}_{ij} = C_{ijkl}\sigma_{kl}; \quad \varepsilon^{u}{}_{ij} = \frac{1}{2}\left(u_{i,j} + u_{j,i}\right) \tag{27}$$

The vector of the nodal d.o.f. for the generic element (e) in its natural reference system ^{J} is thus represented by:

$$\left\{q_e\right\}^T = \left\{\left\{u_i{}^{EM}\right\}_{(e)}, \left\{v_i{}^{EM}\right\}_{(e)}, \left\{w_i{}^{EM}\right\}_{(e)}, \left\{\sigma_{xzi}{}^{J}\right\}_{(e)}, \left\{\sigma_{yzi}{}^{J}\right\}_{(e)}, \left\{\sigma_{zzi}{}^{J}\right\}_{(e)}\right\}^T \tag{28}$$

where $_i$ is the node number (i=1, 8).

Nevertheless the transverse normal stress gradient is not assumed as a functional d.o.f., in order to preserve from stress derivatives as nodal d.o.f., the numerical results will show that the boundary conditions (7) will be spontaneously satisfied since many physical constraints can be point-wise enforced, thus it is sufficient to enforce remaining ones in a weak form to obtain results in a very good agreement with exact solutions, as shown by Icardi and Atzori [48] and Icardi [49] using solid and a layerwise plate elements, respectively. Accurate solutions were obtained either for regular problem involving laminates and sandwiches (even when they are thick and the properties of their constituent layers are distinctly different), or singular problems like the case of a two material wedge with certain side angles and materials with dissimilar properties. Even no case was found where the lack of the enforcement of the continuity of the transverse normal stress gradient gave incorrect results, it could be noticed that this continuity can be accounted for by a suited definition of contributions (13), (13)'.

Hereon the basic steps towards derivation of the present element will be summarized. Details concerning standard aspects will be omitted, being explained in common textbooks. The displacements, represented in synthetic form as D and the interlaminar stresses as S, are interpolated separately as:

$$D = \sum_{1}^{8} D^e N^e_{disp}; \quad S = \sum_{1}^{8} S^e N^e_{stress} \tag{29}$$

since the basic assumption is that the intra-element equilibrium conditions are met in an approximate integral form, thus differently to customary mixed elements the nodal stresses are not required to be represented in a point-wise self-equilibrating form. Accordingly, the same inner representation in x, y can be assumed both for displacements and stresses, i.e. $N^e_{disp} = N^e_{stress} = N$. In the present case, computationally efficient parabolic Lagrange's polynomials are employed. This directly follows form the Hellinger-Reissner governing functional (26), since no second or higher-order derivatives of the primary variables (28) are involved, thus no derivatives of the d.o.f should be chosen as nodal quantities, consequently C^1 or higher-order interpolating functions are unnecessary.

The option of using the same representation was chosen because it makes easier the development of mixed elements without compromising accuracy, as shown since the pioneering papers by Loubignac et al. [39] and Nakazawa [40] and since an identical interpolation for displacements and stresses is acceptable by the viewpoint of numerical stability of mixed elements, as discussed forward.

The present element is not intended for use with nearly incompressible materials, because the mean stresses, i.e. the pressure, are not treated as independent from the total stresses. However, numerical tests demonstrated that accurate results can be obtained in these cases, as shown for a two-material wedge with one half incompressible [48].

The following standard interpolating functions are used for corner nodes (1, 2, 3, 4)

$$N_i = \frac{1}{4}(1-\xi_{0i})(1+(-1)^{i-1}\eta_{oi})(\xi_{oi}\cdot(-1)^{i-1}\eta_{oi}-1) \tag{30}$$

and at mid-side nodes (5, 6, 7, 8)

$$\begin{aligned} N_5 &= \frac{1}{2}(1-\eta_{o5})(1-\xi_{05}{}^2) \\ N_6 &= \frac{1}{2}(1-\eta_{o6}{}^2)(1+\xi_{06}) \\ N_7 &= \frac{1}{2}(1+\eta_{o7})(1-\xi_{07}{}^2) \\ N_8 &= \frac{1}{2}(1-\eta_{o8}{}^2)(1-\xi_{08}) \end{aligned} \tag{31}$$

This parabolic representation is chosen just in order to obtain accurate results with a relatively coarse meshing.

Representations (30) and (31) meets the compatibility condition, as the displacements and the interlaminar stresses are continuous inside and at the edges of the elements. Consistency is also ensured at the interfaces. However, since the membrane stresses are not assumed as nodal d.o.f., they are not continuous across the interfaces, as mentioned above. But this incompatibility should not be removed since the theory of elasticity prescribes that in-plane stresses are discontinuous across the material interfaces. Of course, *z* should be the coordinate in the direction across the layer stack-up, while *x*, *y* lie in a plane parallel to the plane of layers. With this assumption, the stresses within the finite element are represented as:

$$\{\sigma\} = \begin{bmatrix} & & [\hat{D}] & & & \\ \{0\} & \{0\} & \{0\} & \{N_{stress}\} & \{0\} & \{0\} \\ \{0\} & \{0\} & \{0\} & \{0\} & \{N_{stress}\} & \{0\} \\ \{0\} & \{0\} & \{0\} & \{0\} & \{0\} & \{N_{stress}\} \end{bmatrix} \{q_{(e)}\} \tag{32}$$

$[\hat{D}]$ being the matrix that defines the in-plane stress components

$$\{\sigma_{xx} \ \sigma_{yy} \ \sigma_{xy}\}^T = [S^*][B]\{q_{(e)}\} = [\hat{D}]\{q_{(e)}\} \tag{33}$$

$[S^*]$ being the related elastic coefficients and $[B]$ the derivatives of the shape functions.

The "stiffness" matrix is derived in a straightforward, standard way from the internal energy functional U_{HR} substituting the discretized displacements and stresses:

$$\{q_{(e)}\}^T [\hat{K}]^e \{q_{(e)}\} = \{q_{(e)}\}^T \int_V [\hat{C}]^T [B] - \frac{1}{2}[\hat{C}]^T [S][\hat{C}] dV \{q_{(e)}\} \tag{34}$$

while the vector of generalized nodal forces is obtained from the work of forces W_{HR} substituting the finite element discretization of displacements. Assembly of the stiffness matrix and of the vector of nodal forces is carried out with the standard techniques.

The integrals defining the stiffness matrix and the nodal force vector are computed either in exact form using symbolic calculus, so to avoid numerical instabilities, or through Gaussian integration, because a reduced integration scheme could be used (even if it was never applied for obtaining the numerical results given next).

To standardize the computation of integrals, as customarily a topological transformation is carried out from the physical plane (*x, y*) to the natural plane (η, θ) that transforms any quadrilateral element into a square element with unit sides

$$x = \sum_{i=1}^{8} x_i N_i \ \text{ and } \ y = \sum_{i=1}^{8} y_i N_i \tag{35}$$

In this way, the Jacobian matrix

$$[J] = \begin{bmatrix} \frac{\partial x}{\partial \xi} & \frac{\partial y}{\partial \xi} \\ \frac{\partial x}{\partial \eta} & \frac{\partial y}{\partial \eta} \end{bmatrix} \tag{36}$$

necessary for obtaining the physical derivatives $\frac{\partial}{\partial x}$, $\frac{\partial}{\partial y}$ from the derivatives $\frac{\partial}{\partial \xi}$, $\frac{\partial}{\partial \eta}$ over the natural plane

$$\begin{Bmatrix} \frac{\partial}{\partial x} \\ \frac{\partial}{\partial y} \end{Bmatrix} = [J]^{-1} \begin{Bmatrix} \frac{\partial}{\partial \xi} \\ \frac{\partial}{\partial \eta} \end{Bmatrix} \tag{37}$$

can be computed in an efficient way. As well known, stability, solvability and locking phenomena of mixed elements are governed by rather complex mathematical relations (see, Babuska [50] and Brezzi [51]). In particular, certain choices of the shape functions could not yield meaningful results. A necessary condition for solvability, which in most cases suffices for acceptability of mixed elements, is that the number of displacement d.o.f. n_u must be equal (like in the present element), or larger than the number of stress d.o.f. n_σ. A sufficient condition for solvability (see, Olson [52]) is that for a single element that is free of boundary conditions the

number of zero eigenvalues of $[\hat{K}]^e$ is equal to the number of rigid body modes, the total number of positive eigenvalues is equal to the number of stress d.o.f., while the total number of zero and negative eigenvalues is equal to the number of displacement d.o.f. However, even when these admissibility tests are passed, erroneous, highly oscillating results could be obtained. For homogeneous, isotropic materials this problem is usually overcome by relaxing the stress continuity impositions, but in laminated and sandwich composites the interfacial stress continuity conditions cannot be skipped, otherwise the physical meaning of solution is lost. The opposite possibility is that nevertheless these tests are failed, mixed elements could be effective for solving regular problems. Accordingly, mixed elements should be tested considering sample cases with the same features of the practical cases to be solved, whose solution in exact or approximate numerical form is available for comparisons.

In the forthcoming section, solvability, convergence and accuracy tests of the element will be presented, considering laminates and sandwiches with simply-supported and clamped edges, test cases with geometric/material discontinuities and intricate stress variation across the thickness, for which either exact solution in closed-form or in numerical form are available in the literature for comparison.

IV. NUMERICAL APPLICATIONS AND DISCUSSION

Accuracy, convergence and solvability of the present finite element will be assessed comparing its results with exact/numerical solutions of sample test cases available in the literature. Aiming at enhancing the intricacies of stress and displacement fields, cases with strongly asymmetrical lay-ups, clamped edges, distinctly different properties of layers and high face-to-core stiffness ratios will be analysed.

For what concerns the through-the-thickness discretization, please notice that all results presented throughout this section are obtained considering a number of computation layers equal to the number of physical layers, as well as a third order representation of the in-plane displacement and a fourth order representation of the transverse displacement for the contributions of Eq. (3).

4.1 Solvability and convergence

First of all, an eigenvalue solvability test is presented. In accordance with Olson [52], this test is carried out over a single finite element in the shape of a square plate with sides of unit length and free of boundary conditions (thickness should be sufficiently small to have a plane-stress, plane-strain problem). The same isotropic material analysed by Mijuca [53] in a similar test is here considered with the following mechanical properties E_1 (= E_2 = E_3) =1 and υ=0.3. The results of this test are reported in Table 1.

According to the rules discussed above, the finite element shows a number of zero eigenvalues equal to the number of rigid body modes. At the same time, the total number of positive eigenvalues is the same as the number of generalized stress d.o.f. and the total number of zero and negative eigenvalues is equal to the number of generalized displacement d.o.f. These conditions being satisfied in the test, the sufficient condition for solvability is passed by the present mixed element that thus can be applied to solution of other sample cases, in order to verify its behaviour in problems of practical interest.

Aiming at verifying the convergence rate of the present element, the sample case analysed by Zhen et al. [23] is considered, with a length-to thickness ratio of 4. The analysis is carried out for a plate that undergoes a bisinusoidal loading and is simply supported at the edges. The mechanical properties of the constituent material considered for this case are: E_L/E_T=25; G_{LT}/E_T=0.5; G_{TT}/E_T=0.2; υ_{LT}=0.2 and the stacking sequence is [15°/-15°]. Table 2 reports the through-the-thickness variation of the in-plane stress for different meshing schemes by the present element and by Zhen et al. [23], normalised as follows:

$$\bar{\sigma}_x = \frac{\sigma_x\left(\frac{L_x}{2}, \frac{L_y}{2}, z\right) h^2}{p^0 L_x^2}; \tag{38}$$

The results of Table 3 show that the present element is as accurate as the 3D solutions reported in Ref. [23], and even with rather coarse meshing the accuracy is satisfactory. This confirms that mixed elements are accurate without requiring a very fine discretization as already focused in the literature.

As a further assessment of the convergence rate, the laminated [0°/90°/0°] plate for which Vel and Batra computed the exact 3D solution in Ref. [42] is considered. The plate is square and has a length to thickness ratio (L_x/h) of 5. The mechanical properties of the constituent material are the same as in the previous case. For what concerns boundary and loading conditions, the plate is simply supported on two opposite edges, clamped on the other two and it is undergoing a bi-sinusoidal normal load with intensity p^0 on the upper face, whereas the bottom one is traction free. It could be noticed that the structural model can treat clamped edges because a non-vanishing transverse shear resultant can be obtained with all displacement d.o.f. vanishing with

an appropriate choice of variable kinematics contribution Δ^i. The results of Table 3 are normalized according to [42] as:

$$\bar{\sigma}_{xz} = \frac{10 \cdot H \cdot \sigma_{xz}\left(\frac{L_x}{8}, \frac{L_y}{2}, z\right)}{p^0 L_x}; \quad \bar{w} = \frac{100 E_T \cdot h^3}{p^0 L_x^4} w(0,0,z) \tag{39}$$

Like in the previous case, the numbers in square brackets represent the computational time required to perform the analysis on a laptop computer with a 1800 GHz double-core processor and 2.96 GB RAM. The numerical results show that the present finite element provides very accurate results as compared to the exact 3D solution. Also in this case it is shown that even with a rather coarse discretization the accuracy is good.

4.2 Laminates and sandwiches with different boundary conditions

Hereafter different cases of analysis available in the literature are considered in order to exhaustively verify the accuracy of the present mixed element.

4.2.1 Simply supported sandwich beam

Aiming at assessing the capability of present element to smoothly represent the through-the-thickness stress and displacement distributions even when material properties of constituent layers abruptly change, it is considered an extremely thick, simply supported sandwich beam loaded by a sinusoidal transverse loading. Using the present element, the cellular structure of core could be discretized into details, but this is not done because the results used for comparisons have been determined considering the sandwich beam as a sandwich-like, multi-layered, homogenized structure where the core is described as a quite compliant intermediate thick layer and faces as thin, stiff layers. Therefore, it represents for the finite element a laminate having distinctly different properties of layers. Of course, this approach can be considered whenever it is supposed that local buckling phenomena do not occur in the cellular structure, as they cannot be accounted for by the homogenized description adopted. This approach will be used in all the following applications to sandwiches, since it was used also to obtain the reference solutions.

Faces are laminates with stacking sequence (MAT 1/2/3/1/3), where the constituent material have the following mechanical properties: MAT 1: E_1=E_3=1 GPa, G_{13}=0.2 GPa, υ_{13}=0.25; MAT 2: E_1=33 GPa, E_3=1 GPa, G_{13}=0.8 GPa, υ_{13}=0.25; MAT 3: E_1=25 GPa, E_3=1 GPa, G_{13}=0.5 GPa, υ_{13}=0.25. The core is made of MAT4, whose mechanical properties are as follows: MAT 4: E_1=E_3=0.05 GPa, G_{13}=0.0217 GPa, υ_{13}=0.15. The length to thickness ratio of the beam is 4 and the thickness ratios of the constituent layers are $(0.010h/0.025h/0.015h/0.020h/0.030h/0.4h)_s$. Due to the different thickness of constituent layers and to their distinctly different material properties, strong 3D effects rise for this case. However, in order to introduce the further complication of a strong unsymmetry, cases are presented with E_3 modulus of the core and upper face layers reduced by a 10^2 factor. As shown by the exact solution computed in [43] using the technique described in [41], this produces an opposite variation of the transverse shear stress across the upper and lower faces that is problematic to capture in the simulations.

The results for this case reported in Figure 2 are normalized as follows:

$$\bar{\sigma}_{xz} = \frac{\sigma_{xz}(0,z)}{p^0}; \quad \bar{\sigma}_z = \frac{\sigma_z\left(\frac{L_x}{2}, z\right)}{p^0}; \quad \bar{u} = \frac{u(0,z)}{hp^0}; \quad \bar{w} = \frac{w\left(\frac{L_x}{2}, z\right)}{hp^0}; \tag{40}$$

Figure 2 a represents the through-the-thickness variation of the shear stress $\bar{\sigma}_{xz}$ while Figure 2b represents $\bar{\sigma}_z$, and Figure 2c and 2d represent, respectively, the through-the-thickness variation of the in-plane displacement $\bar{u}$, and of the transverse displacement $\bar{w}$. All the results are obtained considering 150 elements over the beam, as shown by the inset reported in Figure 2. In this case, the analysis requires 16 s. The results of Figure 2 show that the present mixed element can obtain results as accurate as the exact 3D solutions even when the constituent material have abruptly changing mechanical properties that determine strong asymmetrical stress and displacement fields, using a reasonably fine mesh.

4.2.2 Simply supported sandwich plate

Still aiming at verifying the accuracy of the present mixed element in describing stress and displacement fields of structure with strong asymmetric effects, it is now considered the sandwich plate for which Brischetto et al. [44] compute the exact 3D solution. In this case, the asymmetry is due to differences between the thickness ratios of upper (symbol us) and lower (symbol ls) faces, which are respectively h_{ls} =h/10; h_{us} =2h/10 with respect to the thickness h of the plate. The thickness ratio of the core (symbol c) is h_c =7h/10. The constituent material has the following mechanical properties: E_{ls}/E_{us}=5/4, E_{ls}/E_c=10^5, ν_{ls}= ν_{us}=ν_c=ν= 0.34.

For what concerns loading and boundary conditions, the plate is simply supported and it is undergoing bi-sinusoidal loading. The plate has a length to thickness ratio $L_x/h=4$ and a length-side ratio $L_y/L_x=3$. Figure 3 reports the comparison between the exact solutions presented in Ref. [44] and the numerical results for what concerns the in-plane displacement and the transverse shear stress computed using the present finite element, normalized as follows:

$$\bar{\sigma}_{xz} = \frac{\sigma_{xz}\left(0, \frac{L_y}{2}, z\right)h}{q^0 L_x}; \quad \bar{u} = \frac{u\left(0, \frac{L_y}{2}, z\right)E_c h^2}{q^0 L_x^3} \tag{41}$$

The results of Figure 3 have been obtained considering 300 elements and modelling only a quarter of the plate (see inset in Figure 3). Also in this case, despite the asymmetry of the structure, the present mixed element can obtain results in a very good agreement with the exact 3D solution at any point with the right gradients at the interfaces, requiring just 35 s to perform the analysis.

4.2.3 Cantilever sandwich beam

In order to more deeply assess whether the present finite element can accurately describe the stress field also with clamped edges, the cantilevered sandwich beam subjected to a uniform transverse loading of Ref. [45] is considered. The beam has laminated faces made of unidirectional Carbon-Epoxy laminates (E_1= 157.9 GPa, $E_2=E_3$= 9.584 GPa, $G_{12}= G_{13}$= 5.930 GPa, G_{23}= 3.277 GPa, $\nu_{12}= \nu_{13}$= 0.32, ν_{23}= 0.49), while the core is made with a PVC foam core (E= 0.1040 GPa, ν= 0.3). According to [45], a length-to-thickness ratio of 10 is assumed, while the thickness ratios of the constituent layers are 0.1h/0.8h/0.1h.

Figure 4 reports the through-the-thickness distribution of the transverse shear stress and the meshing scheme adopted. The stress is normalised as follows:

$$\bar{\sigma}_{xz} = \frac{2h}{L_x p^0}\sigma_{xz}\left(\frac{L_x}{5}, \frac{L_y}{2}, z\right) \tag{42}$$

The results of Figure 4 confirm the accuracy of the present mixed element as it obtains results in good agreement with those by the 3D finite element of Ref. [45]. For what concerns the computational times, only 17.5 s are required to perform the analysis. Thus, even if the model of Eqs. (1) and its EM counterpart have as functional d.o.f. the displacements and the transverse shear rotations at the middle plane, it does not give poor results for clamped structures like the equivalent single-layer models with classical five mid-plane d.o.f., because enforcing the vanishing of displacements at the clamped edges does not necessarily mean that the transverse shear stress resultant also vanishes. Also in this case, quite accurate results are obtained with a not extremely refined meshing.

4.2.4 Cantilever piezo-actuated beam

With the goal of verifying the accuracy of the present mixed element for clamped structure with abruptly changing material properties, the cantilever piezoactuated beam formerly studied by Robbins and Reddy [46] is considered. The structure is made of an underlying aluminium beam substructure (thickness 15.2 mm), an adhesive film (thickness 0.254 mm) and a piezoactuator (thickness 1.52) bonded on the upper face. The material properties of the constituent materials are: E_{alum}=69 GPa, G_{alum}=27.5 GPa, υ_{alum}=0.25; E_{ad}=6.9 GPa, G_{ad}=2.5 GPa, υ_{ad}=0.4; E_{1piezo}=69 GPa, E_{3piezo}=48 GPa, G_{piezo}=21 GPa, $\upsilon_{13piezo}$=0.25, $\upsilon_{31piezo}$=0.175. Piezoactuator, adhesive and aluminium substructure form an unsymmetrical three material laminate that exhibits bending/extension coupling. The only acting loads for this case are the self-equilibrating loads induced by the piezoactuator. A bending deformation is provided by applying an actuation strain of 0.001 to the piezoelectric layer via an applied electric field. The length of the beam is 152 mm.

Figure 5a shows the spanwise variation of membrane, transverse shear and transverse normal stresses near the top of the aluminium substrate (z1= 6.61 mm) and at the centre of the adhesive layer (z2= 6.84 mm), while Figure 5b represents the stress fields across the thickness close to the free edge. The stress distributions are presented in the following normalized form, according to [46], where the exact solution for this case is presented:

$$\bar{\sigma}_x = \frac{A_{tot}\cdot\sigma_x\cdot 10^3}{(E_1A)_{alum}+(E_1A)_{ad}+(E_1A)_{piezo}};$$
$$\bar{\sigma}_z = \frac{A_{tot}\cdot\sigma_z\cdot 10^3}{(E_3A)_{alum}+(E_3A)_{ad}+(E_3A)_{piezo}}; \quad (43)$$
$$\bar{\sigma}_{xz} = \frac{A_{tot}\cdot\sigma_{xz}\cdot 10^3}{(G_{13}A)_{alum}+(G_{13}A)_{ad}+(G_{13}A)_{piezo}};$$

the subscripts *alum*, *ad*, *piezo* and *tot* being used to indicate the cross sectional area and the elastic moduli of the substrate structure, of the adhesive and of the piezoactuator layer, respectively, which are considered as isotropic materials.

The results of Figure 5 show that the present mixed element is accurate also for this case in which a singular-like stress filed arise. In details, in Figure 5a it can be noticed that the element accurately describes the unwanted dangerous stress concentrations that appear at the free end of the beam that could cause debonding of the piezoactuator in service, without showing erroneous oscillating results close to the edge. Also the through-the-thickness distribution of the stresses is well described as shown in Figure 5b, in particular the mixed element is capable to capture the sharp variation of the bending stress that can be seen near the bonding layer also in this case with a reasonably refined meshing. For this case of analysis the present element required 47 s.

4.2.5 Double lap joint with aluminum adherents

As an application to a practical case, it is now considered the joint with aluminium 2024 T3 adherents analysed by Nemes and Lachaud [47]. The adhesive is epoxy resin REDUX 312/5 (E=27 GPa, G=1 GPa, υ=0.35) and it is 0.1 mm thick. The outer layer is 2 mm thick, the inner one is 4 mm thick, and the overlap length is 50 mm. A pressure load in *x* with intensity 1 N/mm is applied to the inner adherent, while the lower and the upper adherents are clamped at right and left bounds.

This case is treated as a plate with step variable properties in the finite element analysis, the adherents being constituted by a homogeneous and isotropic medium, while the overlap is constituted by and a three-layer laminate. Of course, all continuity functions vanish in the adherents, while they exist at the two interface between adhesive and lower adherent, adhesive and upper adherent. The piecewise contributions of Eqs. (13) – (13') are considered in this case in order to make continuous the stresses and their gradients at the interface of adherents and overlap, where properties vary from a single layer to a three-layer plate. Specifically, the terms of first order are aimed at fulfilling the continuity of the stresses; those of second order are aimed at satisfying the continuity of the stress gradients. The variable kinematic contributions across the thickness (3) in this case are aimed at satisfying also the stress boundary conditions at the ends of the overlap Ω_1, Ω_2:

$$N = \int_{\Omega_i}\sigma_{xx}dz = -\int_{\Omega_i}\sigma_{xz}dx; \quad M = \int_{\Omega_i} z\,\sigma_{xx}dz; \quad Q = \int_{\Omega_i}\sigma_{xz}dz; \quad (44)$$

N, *M*, *Q* being the in-plane, bending and shear resultants, respectively, along with the stress-free boundary conditions

$$\sigma_{xz} = 0; \quad \int_{\Omega_i}\sigma_{xz}dz = 0; \quad \sum_k \int_{\Omega_k}\sigma_{xz}dz = 0;$$
$$\sigma_{xx} = 0; \quad \int_{\Omega_i}\sigma_{xx}dz = 0; \quad \sum_k \int_{\Omega_k}\sigma_{xx}dz = 0; \quad (45)$$

at the free edges of the overlap. The results for this case are presented in Figure 6, where the in-plane variations of the peel stress and of the shear stress are reported. They are obtained requiring 69 s to perform the analysis and modelling the whole joint with 600 elements with 2 concentrations of elements across the variation of adherents, as shown by the inset. Also this case confirms the accuracy of the mixed element, which correctly describes the stress peaks near the end of the overlap, which can have detrimental effects on the service life of the joint.

V. CONCLUDING REMARKS

A quadrilateral, eight-node, mixed plate element for analysis of laminates with general lay-up and sandwich composites with high face-to-core stiffness ratios and distinctly different properties of top and bottom faces, was developed. It has the displacements and the interlaminar stresses at the reference mid-plane as nodal d.o.f. Its structural model is a 3D physically based zig-zag one with fixed functional d.o.f. (the three displacements and the two transverse shear rotations at the mid-plane), whose representation can be refined across the thickness without increasing the unknowns. This model also allows the material properties to suddenly vary in the in-plane directions. A piecewise variable transverse displacement is assumed, since it has a significant bearing for certain problems, e.g. when temperature gradients cause thermal stresses, for the crushing

behaviour of sandwiches, around geometric and material discontinuities and close to loading points. The expressions of continuity functions and higher-order coefficients of displacements incorporated in order to a priori satisfy all the physical constraints are determined once for all in closed-form as expressions of the five d.o.f. and of their spatial derivatives using a symbolic calculus tool.

The energy updating technique (SEUPT) is used to convert the d.o.f. derivatives without resulting in an increased number of variables. It allows obtainment of an equivalent C^0 version of the zig-zag model that is used to develop the finite element. The three displacements and the three interlaminar stresses at the mid-plane are assumed as nodal d.o.f. All these quantities are interpolated using the same standard serendipity shape functions because this simplifies the development of the element without resulting in any accuracy loss, as shown by the comparison with exact solutions of sample cases. Consequently, equilibrium equations are satisfied just in approximate integral form.

Accuracy, solvability and convergence were assessed considering multi-layered monolithic structures with cross-ply and angle-ply lay-up and sandwich-like structures with also abruptly changing properties of faces, with different loading and boundary conditions, for which exact solutions are available. The structural model and the mixed formulation make easier the enforcement of stress-boundary conditions, either because the coefficients of higher-order terms can be determined from enforcement of these conditions, or the stresses are nodal variables. An application was presented also to an adhesively bonded joint, which represents a case with step varying properties, the adherents and the overlap being seen as interfaced plates with a different lay-up. The element was shown to be fast convergent and its results were not affected by the mesh configuration, as accurate predictions were obtained also with rather coarse meshes. It appears as a good alternative to the ones to date available in the literature, as it offers a good accuracy with the minimal number of unknown nodal variables at an affordable cost.

REFERENCES

[1]. J. Sliseris, K. Rocens K. Optimal design of composite plates with discrete variable stiffness. Composite Structures, 98: 15 – 23, 2013.

[2]. J. Barth. Fabrication of complex composite structures using advanced fiber placement technology. In Proc. 35th International SAMPE Symposium, 35, pages 710-720Anaheim, CA 1990.

[3]. C.S. Sousa, P.P. Camanho, A. Suleman. Analysis of multistable variable stiffness composite plates. Composite Structures, 98: 34 – 46, 2013.

[4]. S. Honda, T. Igarashi, Y. Narita, Multi-objective optimization of curvilinear fiber shapes for laminated composite plates by using NSGA-II. Composites: Part B, 45: 1071 – 1078, 2013.

[5]. D. Càrdenas, H. Elizalde, P. Marzocca, F. Abdi, L. Minnetyan, O. Probst. Progressive failure analysis of thin-walled composite structures. Composite Structures 95: 53-62, 2013.

[6]. A. Chakrabarti, H.D. Chalak, M.A. Iqbal, A.H. Sheikh, A new FE model based on higher order zig-zag theory for the analysis of laminated sandwich beam soft core. Composite Structures 93: 271-279, 2011.

[7]. M.S. Qatu, R.W. Sullivan, W. Wang, Recent research advances on the dynamic analysis of composite shells: 2000-2009, Composite Structures 93: 14-31, 2010.

[8]. Y. Zhang, C. Yang, Recent developments in finite element analysis for laminated composite plates. Composite Structures 88: 147-157, 2009.

[9]. H. Matsunaga, A comparison between 2-D single-layer and 3-D layerwise theories for computing interlaminar stresses of laminated composite and sandwich plates subjected to thermal loadings. Composite Structures 64: 161-177, 2004.

[10]. W.J. Chen, Z. Wu, A selective review on recent development of displacement-based laminated plate theories. Recent Pat. Mech. Eng., 1: 29–44, (2008).

[11]. I. Kreja, A literature review on computational models for laminated composite and sandwich panels. Central European Journal of Engineering, 1: 59 – 80, 2011.

[12]. M. Tahani, Analysis of laminated composite beams using layerwise displacement theories. Composite Structures, 79: 535-547, 2007.

[13]. M. Gherlone, On the use of zigzag functions in equivalent single layer theories for laminated composite and sandwich beams: a comparative study and some observations on external weak layers. J. of Appl. Mech., 80, 2013.

[14]. E. Carrera, F. Miglioretti, M. Petrolo, Accuracy of refined finite elements for laminated plate analysis. Composite Structures, 93: 1311-1327, 2011.

[15]. R.P. Shimpi, A.V. Ainapure, A beam finite element based on layerwise trigonometric shear deformation theory. Composite Structures, 53: 153-162, 2011.

[16]. D. Elmalich, O. Rabinovitch. A higher-order finite element for dynamic analysis of soft-core sandwich plates. J. Sandwich Struct. & Mat., 14: 525-555, 2012.

[17]. F. Dau, O. Polit, M. Touratier. C^1 plate and shell elements for geometrically nonlinear analysis of multi-layered structures. Composite Structures, 84: 1264-1274, 2006.

[18]. S.V. Hoa, W. Feng. Hybrid finite element method for stress analysis of laminated composites. Kluwer Academic Publ., 1998.

[19]. W. Feng, S.V. Hoa. Partial hybrid finite elements for composite laminates. Finite Elements in Analysis and Design, 30: 365-382, 1998.

[20]. Y.M. Desai, G.S. Ramtekkar, A.H. Shah. Dynamic analysis of laminated composite plates using a layer-wise mixed finite element model. Composite Structures, 59: 237-249, 2003.

[21]. G.S. Ramtekkar, Y.M. Desai, A.H. Shah. Application of a three-dimensional mixed finite element model to the flexure of sandwich plate. Comp. & Struct., 81: 2183-2198, 2003.

[22]. C.W.S To, M.L. Liu. Geometrically nonlinear analysis of layerwise anisotropic shell structures by hybrid strain based lower order elements. Finite Elements in Analysis and Design, 37: 1-34, 2001.

[23]. W. Zhen, S.H. Lo, K.Y. Sze, C. Wanji. A higher order finite element including transverse normal strain for linear elastic composite plates with general lamination configurations. Finite Elements in Analysis and Design, 48 :1346 – 1357, 2012.
[24]. C. Cao, A. Yu, Q.-H. Qin. A novel hybrid finite element model for modelling anisotropic composites, Finite Elements in Analysis and Design 64: 36 – 47, 2013.
[25]. P. Dey, A.H. Sheikh, D. Sengupta. A new element for analysis of composite plates. Finite Elements in Analysis and Design, 82: 62 – 71, 2014.
[26]. J.N. Reddy. Mechanics of Laminated Composite Plates and Shells: Theory and Analysis. CRC Press, 2003.
[27]. M. Di Sciuva. Development of an Anisotropic, Multilayered, Shear-Deformable Rectangular Plate Element. Composite Structures, 21: 789–796, 1985.
[28]. C.N. Phan, Y. Frostig, G.A. Kardomateas. Free vibration of unidirectional sandwich panels, Part II: Incompressible core. J. Sandwich Struct. & Mat., 15: 412-428, 2013.
[29]. V.R. Aitharaju, R.C. Averill. C0 zig-zag finite element for analysis of laminated composites beams. J. of Eng. Mech., 125: 323-330, 1999.
[30]. X.Y. Li, D. Liu. Generalized laminate theories based on double superposition hypothesis. Int. J. Num. Meth. Eng., 40, 1197–212, 1997.
[31]. W. Zhen, C. Wanji. A C0-type higher-order theory for bending analysis of laminated composite and sandwich plates. Composite Structures, 92: 653–661, (2010).
[32]. M. Cho, K.O. Kim, M.H. Kim. Efficient higher-order shell theory for laminated composites. Composite Structures, 34: 197–212, 1996.
[33]. R. Sahoo, B.N. Singh. A new shear deformation theory for the static analysis of laminated composite and sandwich plates. Int. J. of Mech. Sci., 75: 324-336, 2013.
[34]. U. Icardi, F. Sola. Development of an efficient zig-zag model with variable representation of displacement across the thickness. J. Eng. Mech., 140: 531-541, 2014.
[35]. U. Icardi. Multilayered plate model with "adaptive" representation of displacements and temperature across the thickness and fixed d.o.f. Journal of Thermal Stresses, 34: 958–984, 2011.
[36]. U. Icardi. C^0 plate element based on strain energy updating and spline interpolation, for analysis of impact damage in laminated composites. International Journal of Impact Engineering, 34: 1835–1868, 2007.
[37]. U. Icardi. Extension of the Strain Energy Updating Technique to a multilayered shell model with adaptive displacements and fixed DOF. J. Aerosp. Eng., 26: 842-854, 2013.
[38]. U. Icardi, F. Sola. C0 layerwise model with fixed d.o.f. and variable in and out-of-plane kinematics by SEUPT. Int. J. of Research Studies in Science, Engineering and Technology (IJRSST) IN PRESS
[39]. C. Loubignac, C. Cantin, C. Touzot. Continuous stress fields in finite element analysis. AIAA Journal, 15: 1645-1647, 1978.
[40]. S. Nakazawa. Mixed finite elements and iterative solution procedures. Iterative Methods in Non-Linear Problems. Pineridge, 1984.
[41]. N.J. Pagano. Exact solutions for composite laminates in cylindrical bending. J. Compos. Mater. 3, 398–411, 1969.
[42]. S.S. Vel, R.C. Batra. Analytical solution for rectangular thick laminated plates subjected to arbitrary boundary conditions. AIAA J., 11: 1464-1473, 1999.
[43]. U. Icardi. Higher-order zig-zag model for analysis of thick composite beams with inclusion of transverse normal stress and sublaminates approximations. Composites: Part B, 32: 343-354, 2001.
[44]. S. Brischetto, E. Carrera, L. Demasi. Improved response of asymmetrically laminated sandwich plates by using Zig-Zag functions. J. of Sand. Structures and Materials, 11: 257- 267, 2009.
[45]. A. Tessler, M. Di Sciuva, M. Gherlone. Refined zig-zag theory for laminated composite and sandwich plates. Technical Report No. TP-2009-215561, NASA, Langley, VA, 2009.
[46]. D.H. Robbins, J.N. Reddy. Analysis of piezoelectrically actuated beams using a layer-wise displacement theory. Comp. & Struct., 41: 265–279, 1991.
[47]. O. Nemes, F. Lachaud. Double-lap adhesive bonded-joints assemblies modeling. Int. J. of Adhesion and Adhesives, 30: 288-297, 2010.
[48]. U. Icardi. A. Atzori. Simple, efficient mixed solid element for accurate analysis of local effects in laminated and sandwich composites. Advances in Eng. Software, 32: 843-849, 2004.
[49]. U. Icardi. Layerwise mixed element with sublaminates approximation and 3D zig-zag field, for analysis of local effects in laminated and sandwich composites. Int. J. for Num. Meth in Eng, 70: 94-125, 2007.
[50]. I. Babuska. The finite element method with Lagrange multipliers. Numerical Mathematics, 20: 179-192, 1973.
[51]. F. Brezzi. On the existence, uniqueness and approximation of saddle point problems arising from Lagrangian multipliers. Revue Francaise D'Automatique, Informatique, Recherche Operationelle, Analyse Numerique, 8: 129-151, 1974.
[52]. M.D. Olson. In Hybrid and mixed finite element methods, Atluri SN, Gallagher RH, Zienkiewicz OC, John Wiley & Sons, 1983, 19-49.
[53]. D. Mijuca. A new primal-mixed 3D finite element. The Scientific Journal Facta Universitatis, Mechanics, Automatic, Control and Robotics, 3: 167–178, 2001.

Mode	Eigenv.	Mode	Eigenv.	Mode	Eigenv.	Mode	Eigenv.
1	2	5	0.2142	9	0	13	-0.3015
2	0.8999	6	0.1795	10	0	14	-0.6435
3	0.6364	7	0.1445	11	0	15	-0.6988
4	0.456	8	0.0557	12	-0.2326	16	-2.0244

Table 1. Solvability test for an isotropic material

z/h	-0.5	-0.2	0.0^-	0.0^+	0.2	1
3D [23]	-0.9960	-0.0373	0.4526	-0.4719	0.0260	1.0446
Zhen et al. [23] 4x4	-1.0292	-0.0371	0.4719	-0.4926	0.0240	1.0812
Present 4x4 [2.33]	-1.0291	-0.0371	0.4721	-0.4924	0.0250	1.0791
Zhen et al. [23] 8x8	-0.9992	-0.0356	0.4582	-0.4771	0.0235	1.0481
Present 8x8 [8.51]	-0.9991	-0.0362	0.438	-0.4751	0.0239	1.0465
Zhen et al. [23] 12x12	-0.9925	-0.0353	0.4552	-0.4738	0.0234	1.0411
Present 12x12 [17.1]	-0.0995	-0.0372	0.4531	-0.4729	0.0249	1.0451
Zhen et al. [23] 14x14	-0.9910	-0.0353	0.4546	-0.4732	0.0234	1.0396
Present 14x14 [20.2]	-0.9961	0.0374	0.4525	-0.4718	0.0261	1.0446

Table 2. Normalised in plane stress for a [15°/-15°] square plate by Zhen et al. [23]and by the present mixed element with progressively refining meshing.

	z/h	-0.50	-0.40	-0.30	-0.20	-0.10	0.00	0.10	0.20	0.30	0.40	0.50
$\bar{\sigma}_{xz}$	Ref. [42]	0.000	2.609	3.227	2.643	2.113	2.093	2.100	2.668	3.340	2.734	0.000
	Present (3x3) [1.97]	0.000	2.720	3.830	2.949	2.450	2.360	2.450	2.950	3.950	2.920	0.000
	Present (5x5) [2.70]	0.000	2.650	3.450	2.734	2.325	2.248	2.299	2.750	3.430	2.805	0.000
	Present (9x9) [9.26]	0.000	2.607	3.227	2.643	2.114	2.094	2.099	2.668	3.340	2.735	0.000
$\bar{w}$	Ref. [42]	1.152	1.158	1.162	1.167	1.173	1.180	1.188	1.198	1.208	1.218	1.227
	Present (3x3)	1.613	1.545	1.450	1.406	1.375	1.340	1.333	1.388	1.398	1.415	1.443
	Present (5x5)	1.234	1.288	1.291	1.299	1.304	1.306	1.309	1.295	1.299	1.305	1.312
	Present (9x9)	1.153	1.158	1.161	1.168	1.172	1.180	1.188	1.197	1.207	1.217	1.228

Table 3. Normalised shear stress and transverse displacement for a [0°/90°/0°] square plate by Vel and Batra [42] (exact 3D solution) and by the present mixed element with progressively refining meshing.

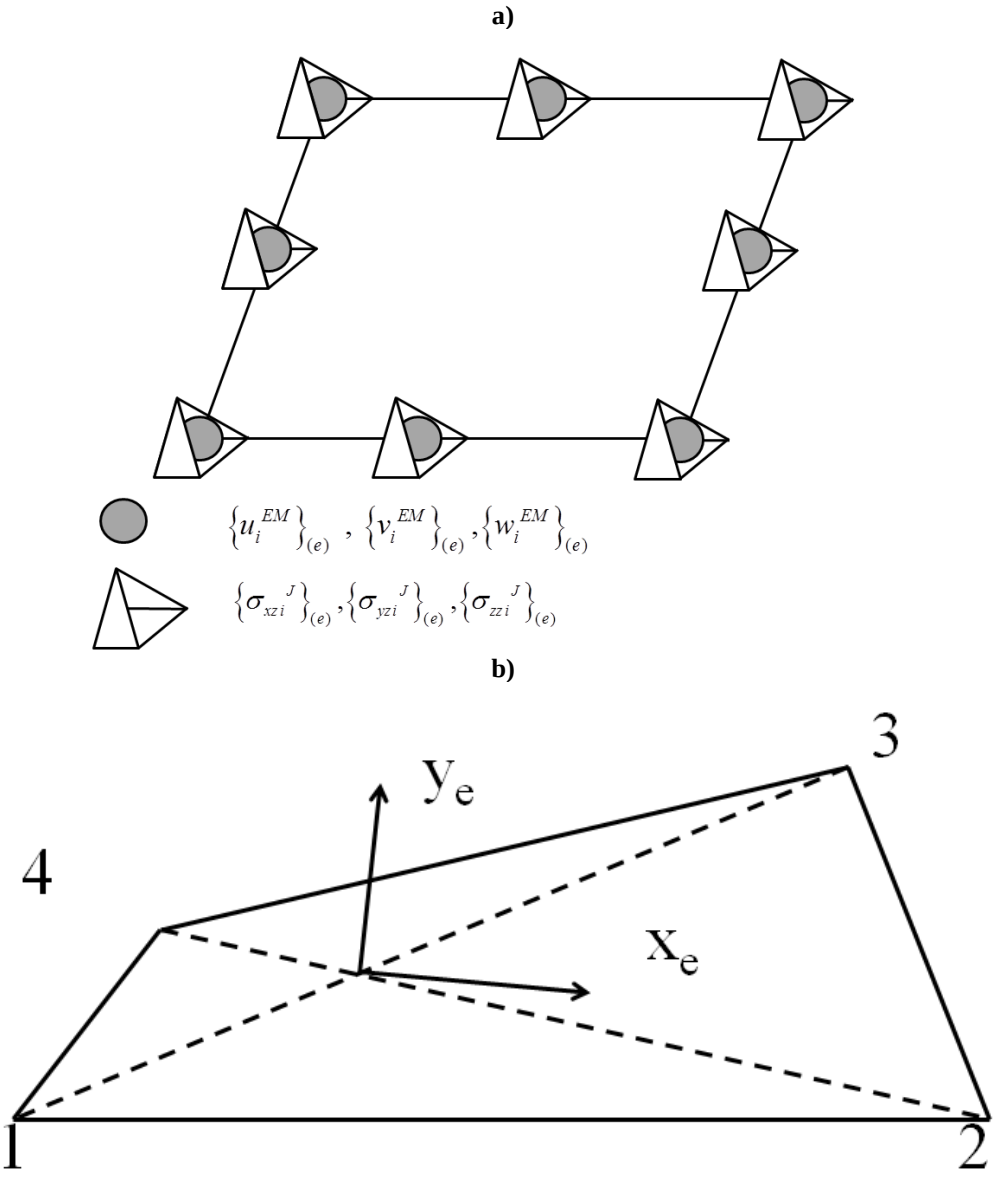

Figure 1. Reference system for the element in: a) the natural plane and b) the physical plane.

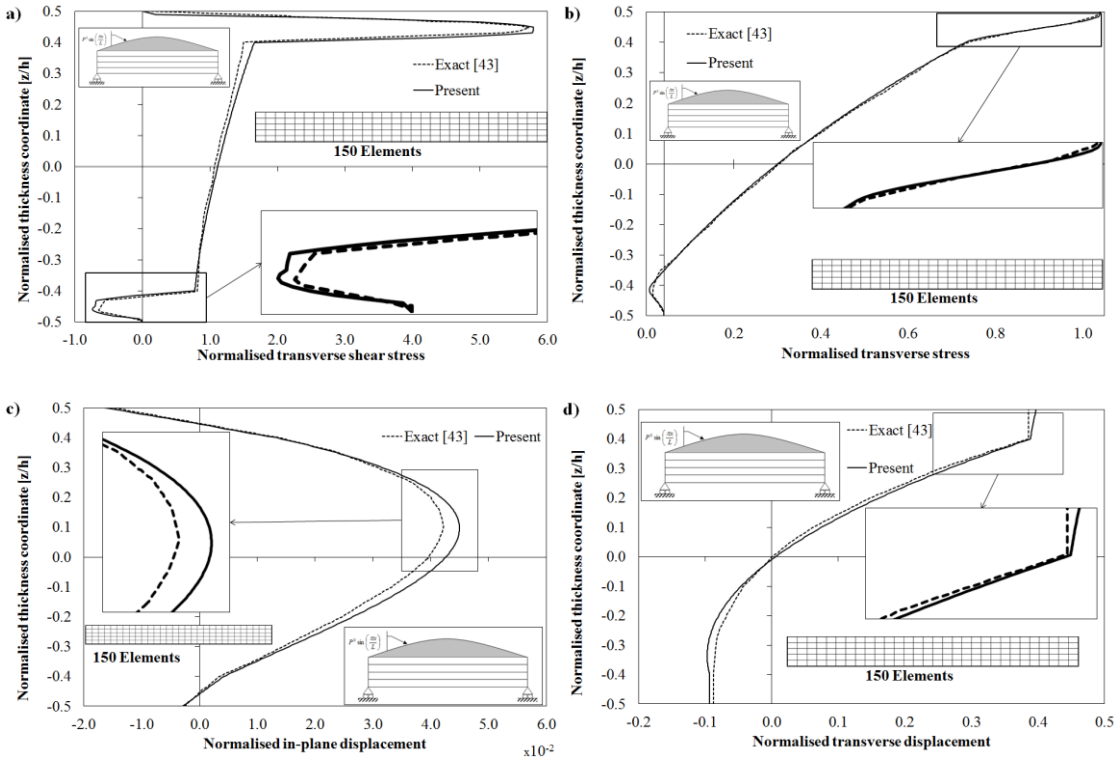

Figure 2. Stress and displacement field by the present mixed element and exat 3D solution [43] for a sandwich beam.

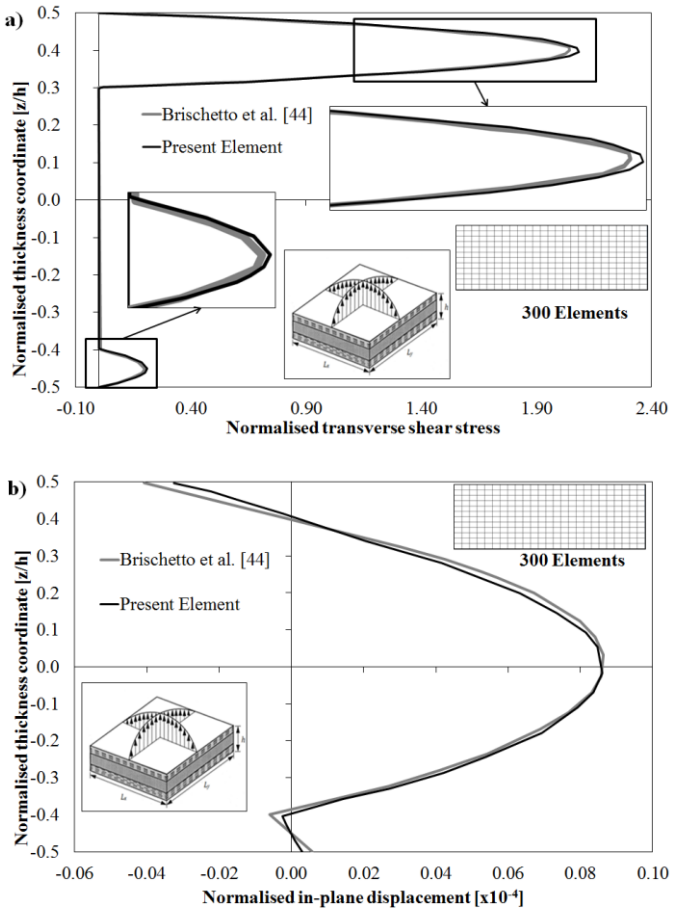

Figure 3. Transverse shear stress and in-plane displacement by the present mixed element and by Brischetto et al. [44] (Exact solution) for a simply supported sandwich plate.

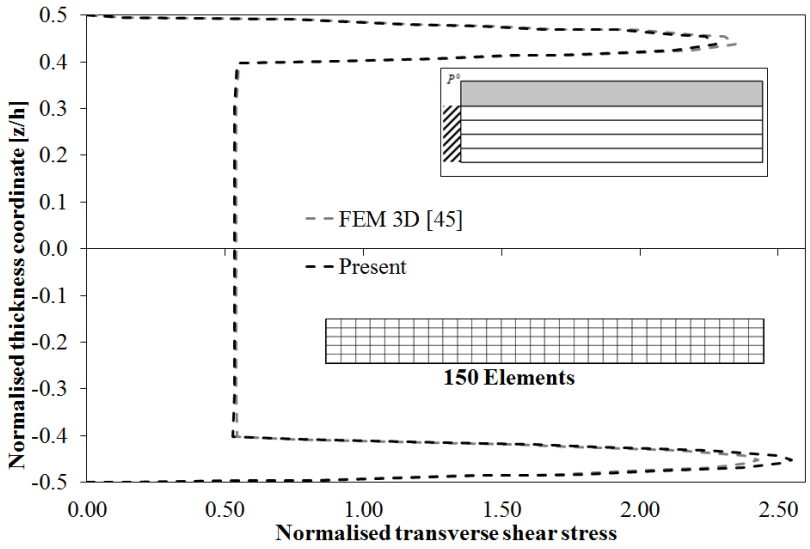

Figure 4. Normalised transverse shear stress by the present mixed element and by the 3D finite element by Tessler at al. [45]

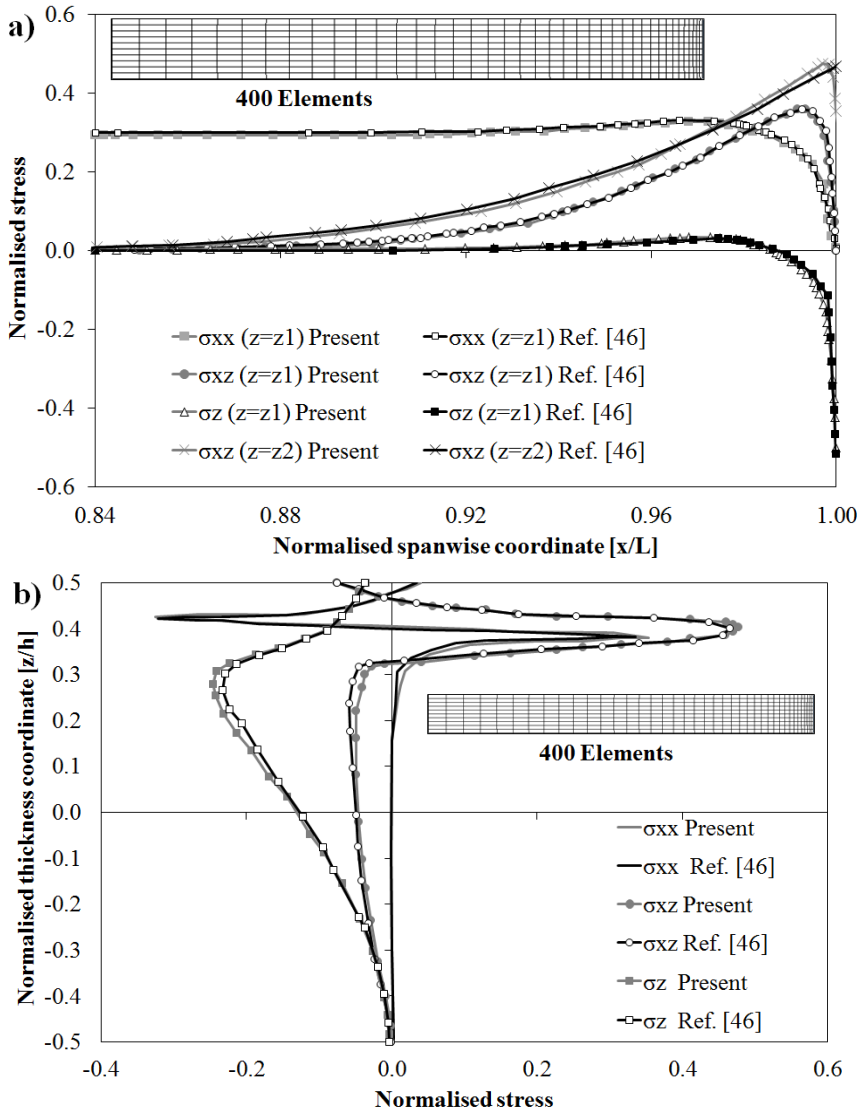

Figure 5. Normalised variation of the stress field for a cantilever piezoactuated beam a) along the span and b) across the thickness

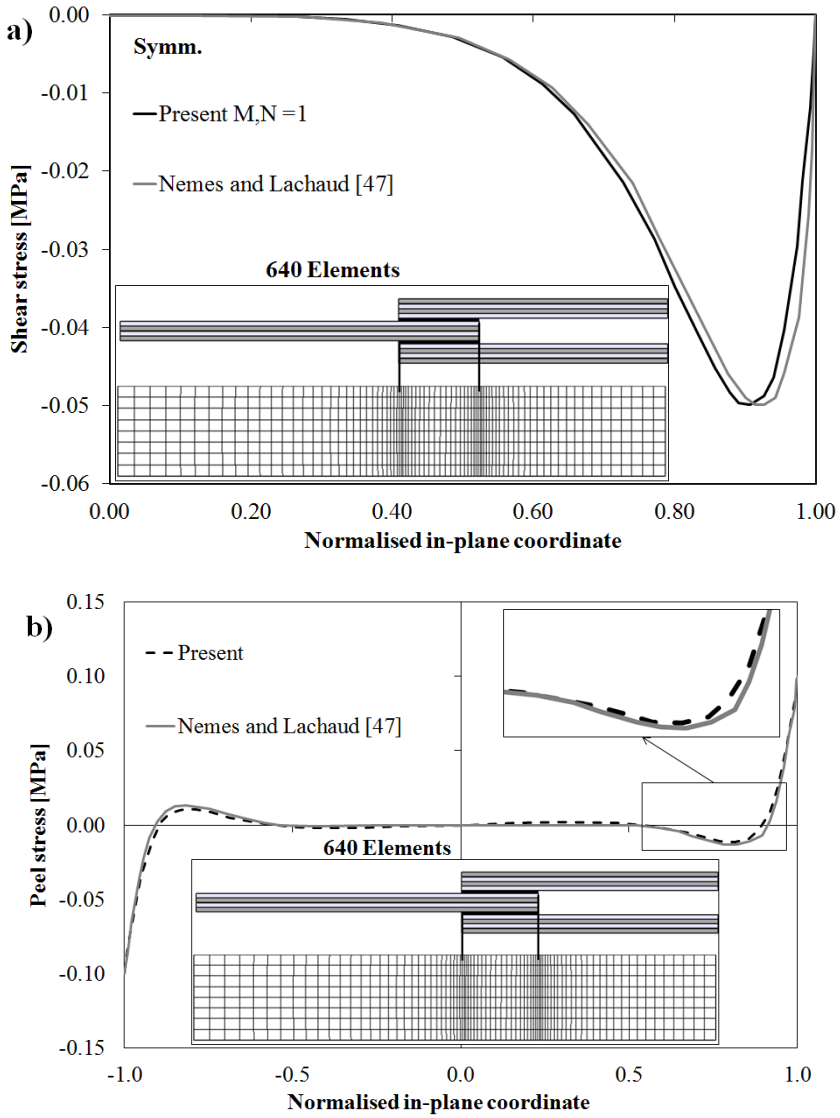

Figure 6. Span-wise distribution of a) shear stress and b) peel stress by Nemes and Lachaud [47] and by the present model